Optimization of Drop Characteristics in a Carrier Cooled Gas Stream using ANSYS and Globalizer Software Systems on the PNRPU High-Performance Cluster*

Stanislav L. Kalyulin (ORCID 0000-0002-5998-0950)[1], Evgenya V. Shavrina[1], Vladimir Ya. Modorskii (ORCID 0000-0002-4200-3440)[1], Konstantin A. Barkalov (ORCID 0000-0001-5273-2471)[2], and Victor P. Gergel (ORCID 0000-0002-4013-2329)[2]

[1]Perm National Research Polytechnical University, Perm, Russia
{ksl, modorsky}@pstu.ru
[2]Lobachevsky State University of Nizhny Novgorod, Nizhny Novgorod, Russia
{konstantin.barkalov, victor.gergel}@itmm.unn.ru

Abstract. We describe in this article the optimization calculations of spray droplets in a gas injected through a nozzle into a work area, as a part of a research of icing on model objects in a small-size climatic wind tunnel. Calculations were performed in a 3D-statement. It is assumed that the drop has some speed, temperature and diameter as it enters the gas flow, which has a specified speed and temperature, so that definite temperature limits are attained when it interacts with a remote obstruction. We determined the maximum gas flow temperature, which corresponds to the minimum of cooling energy consumption. The optimization was carried out using the Globalizer software (Lobachevsky State University of Nizhny Novgorod). Also, we could solve the integration issue between Globalizer and ANSYS Workbench 13.0. ANSYS was employed as a tool to calculate optimization criteria values, whereas Globalizer was used as an optimal parameter search tool. Calculations were performed on the PNRPU high-performance cluster (with a peak performance of 24 TFLOPS).

Keywords: small-size climatic wind tunnel, global optimization, multi-extremal functions, parallel algorithms, droplets flying, numerical simulation, gas flow.

1 Introduction

An energy-efficient [2] closed-loop small-sized climatic wind tunnel (CWT) is being developed at Perm National Research Polytechnical University (PNRPU) [1] with a view to continue scientific investigations into the field of aircraft

* This study was supported by the Russian Science Foundation, project No. 16-11-10150.

aerodynamics. This installation which will provide an opportunity to conduct aerodynamic experiments with simulated in-flight icing conditions at flow Mach numbers as high as $M = 0.8$ and stagnation temperatures up to 30°C [3].

As it is known, tests in wind tunnels can help to solve the following problems [4]:

1. Investigation of the influence of the gas-streamlined object shape on the object aerodynamic characteristics depending on flow velocity and the body position in space.
2. Investigation of air machines: gas turbines, compressors, propellers, windmills, fans, etc.
3. Investigation of engine characteristics (piston turbojet, ramjet, etc.).
4. Investigation of aircraft flight dynamics.
5. Investigation of the influence of aerodynamic forces on the elasticity of aircraft structures (e.g., research into aircraft wing flutter).
6. Physical investigations related to air flow under different conditions (research into the boundary layer, supersonic flows, spatial streams, etc.).
7. Methodical and scientific investigations related to the creation of wind tunnels as physical facilities, test method development in tunnels and processing of the results obtained.

The article discusses the design of an energy-efficient closed-loop small-sized CWT for full-scale icing simulation. The modeling of this process requires structural elements such as air-cooling system, injectors for water supply to the tunnel, a device to heat them, and a dehumidifying system (described in the patent [5]).

A distinctive feature of the design is its high energy efficiency, which will allow for testing under icing conditions at a much lower cost than already existing large testing facilities. This economy is achieved through its ability to consume only the energy required in operating mode to maintain a predetermined level of air flow and by reducing the characteristic dimensions of the CWT [3].

According to studies by Russian scientists [6], the contour of the CWT must be open, so that moisture does not accumulate. The working part is enclosed as its length is enough to equalize the drop temperature to air temperature. Owing to the fact that large CWTs are energy-intensive installations, small-size models are becoming more popular. However, scale model sizes less than 1 : 8 lead to distortion of the icing shape, which is unacceptable. Thus, there is a limitation on the minimum diameter of the CWT.

Given the large time and material costs that are necessary for the preparation and execution of physical experiments in an energy-efficient closed-loop small-sized CWT, numerical simulation of experiments has become the most popular method for studying icing processes. We propose the joint use of numerical and physical experiments.

Ice formation processes during field experiments (spraying water with subsequent freezing) determine three tasks that must be accomplished for the numerical simulation of processes occurring in a CWT:

1. Simulation of cooling gas flowing in the CWT.
2. Simulation of drop disintegration to determine correctly the size of ice particles.
3. Simulation of the "water-ice" phase transition.

ANSYS CFX numerical experiments concerning spraying of water particles are possible with the use of different mathematical models of various degrees of accuracy. In most cases, however, significant computational resources are required.

A modeling of icing was performed in [7], but the method suggested by the authors does not allow to model the characteristics of the surface roughness, nor complex-shaped ice build-ups (such as the unevenness of the "lobster tail") in icing areas at small slip angles of the drops. According to [8], small build-ups of this kind have a more significant impact than the "horn-shaped" ones. Also, that paper discusses a technique that allows to estimate the probability of such ice build-ups. It is not possible, however, to obtain sufficiently accurate data on the nature of the build-ups in such processes as flow separation from a wing.

Icing simulation in ANSYS FENSAP-ICE has not gained much popularity due to requirements to conclude additional license agreements and an insufficient number of validation studies. Nevertheless, a solution example of the problem of icing in ANSYS FENSAP-ICE in conjunction with ANSYS CFX was presented by researchers from Louisiana in [9]. ANSYS CFX and ANSYS FLUENT gas dynamics packages are usually used in this regard in research practice.

As a rule, information on temperature, humidity, speed and other gas dynamics parameters are used to predict icing, since a direct modeling of the "water-ice" phase transition is not possible in these packages. Besides, investigations on gas dynamics problems performed abroad with the use of the ANSYS CFX and ANSYS FLUENT packages relied on subsequent accurate gas dynamics parameters to solve the problem of icing by semi-empirical or analytical methods [10].

The statement of the problem of numerical simulation depends on the type of icing, which can be divided into four categories [6, 11, 12]:

1. The roughness of the ice surface surpasses the height of the local boundary layer, affecting not only the transition of the boundary layer to a turbulent state, but also its separation downstream.
2. The icing is characterized by grooves along the stream. In this case, the area of flow separation primarily depends on the attack angle. In combination with its roughness, this type of icing mainly affects the increase in resistance.
3. In some cases, the droplets spreading over the surface crystallize immediately. Then the ice begins to grow in a vicinity of the critical point adopting the shape of a "horn". In other cases, crystallization is delayed; a film of water creeps over the surface, and ice forms along two areas on the side of the critical point, forming two "horns". The icy "horns" create a large separated region which affects aerodynamics. This is accompanied by the separation of flow depending on their shape, position, and angle of attack. It significantly reduces the aircrafts load-bearing properties.

4. When a thermal anti-icing system is working, a film of water moves across the surface to the outer boundary of the heated region and then freezes in the form of a so-called barrier ice. An obstacle is formed which leads to the appearance of a large separated region in front and behind. This significantly affects the aerodynamic characteristics depending on the position and geometry of the obstacle [12].

The nature of these phenomena and the conditions producing a particular type of icing have not been thoroughly studied until now.

Furthermore, the estimation of the surface tension of small droplets with a typical diameter of 20 μm have shown that the excess pressure, which could affect the freezing point of water and the crystallization process, is so small that it practically does not affect the freezing temperature of water [6]. The surface tension only has an effect on the spreading of drops when they hit the surface and the disintegration of the liquid into drops at being expelled from the injectors [13]. These processes are poorly understood and will be the subject of forthcoming experimental studies in CWT.

In this regard, mathematical modeling of icing at the moment is not perfect. Therefore, physical experiments cannot be completely excluded from consideration. Thus, to maximize at present the effectiveness of research into icing processes, both numerical and physical experiments are equally needed.

Investigations are frequently limited to finding one or several solutions that satisfy the requirements of technical specifications. Searching for an optimal solution is usually not possible, since it requires large computational resources.

Therefore, the numerical search for optimal solutions in an acceptable time frame is one of the most important tasks [14, 15]. It increases the quality of decisions and enhances the benefits of numerical calculations, enabling the identification of new dependencies.

2 Gas dynamics problem

2.1 A physical model of the gas dynamics problem

In the physical statement of the problem, it is assumed that a drop with a given velocity, temperature and diameter falls into a gas dynamic flow having some speed and temperature, so that, upon contact with a distant obstacle, certain temperature limits are attained [16]. The distance to the obstacle is equal to 2 m. The maximum temperature of the carrying gas dynamic flow is determined, and it corresponds to the minimum energy consumption of the energy-efficient closed-loop small-sized CWT when it cools.

The calculation is carried out in a 3D dynamic statement. The internal CWT volume is modeled, and the two-phase environment, gravity and interaction with the cooling gas dynamic flow are taken into account.

2.2 Mathematical model of the gas dynamics problem

We applied the finite volume method for the numerical simulation of the drop flight from the site of injection through the nozzle to the working area of the CWT. This implies that the field of the gas dynamic flow is approximated by a finite number of calculation points.

A mathematical model is developed in accordance with the adopted physical model. This model is based on the mass, momentum and energy conservation laws, and is closed with the state equations of an ideal compressible gas and turbulence, as well as with initial and boundary conditions. The mathematical model of the gas dynamics problem includes the following relations [17]:

- The equation of mass conservation for the gas:

$$\frac{\partial}{\partial t}(\rho_{\text{air}}) + \bar{\nabla} \cdot (\rho_{\text{air}} V_{\text{air}}) = Q_{\text{mass}}^{\text{drop}}, \tag{1}$$

  where ρ_{air} is the air density, V_{air} is the air velocity vector, and $Q_{\text{mass}}^{\text{drop}}$ is a source term expressing the increase in weight caused by evaporation of water from the drop surface.
- The equation of momentum conservation for the gas:

$$\frac{\partial}{\partial t}(\rho_{\text{air}} V_{\text{air}}) + (\rho_{\text{air}} V_{\text{air}} \cdot \bar{\nabla}) \cdot V_{\text{air}} = -\bar{\nabla} P + \bar{\nabla} \tau_{\text{air}} + \rho_{\text{air}} g + Q_{\text{force}}^{\text{drop}}, \tag{2}$$

  where P is pressure, g is the gravity vector, τ_{air} is the shear stress at the wall, and $Q_{\text{force}}^{\text{drop}}$ is a source term that expresses the force with which the drop acts on the air.
- The equation of energy conservation for the gas:

$$\frac{\partial}{\partial t}(\rho_{\text{air}} H_{\text{air}}) + \bar{\nabla} \cdot (\rho_{\text{air}} V_{\text{air}} H_{\text{air}}) = \frac{\partial P}{\partial t} \cdot \bar{\nabla} \cdot \left(\left(\frac{\lambda_{\text{air}}}{c_{p_{\text{air}}}} + \mu_t \right) \bar{\nabla} H_{\text{air}} \right) + Q_{\text{energy}}^{\text{drop}}, \tag{3}$$

  where H_{air} is the total enthalpy of the air, λ_{air} is the coefficient of thermal conductivity of the air, $c_{p_{\text{air}}}$ is the air heat capacity, μ_t is turbulent dynamic viscosity, $Q_{\text{energy}}^{\text{drop}}$ is a source term expressing energy transfer between the phases.
- The equation of mass conservation for the steam:

$$\frac{\partial}{\partial t}(\rho_{\text{air}} Y_{\text{steam}}) + \bar{\nabla} \cdot (\rho_{\text{air}} V_{\text{air}} Y_{\text{steam}}) = \bar{\nabla} \cdot \left(\left(\rho_{\text{air}} D + \frac{\mu_t}{S_{c_t}} \right) \bar{\nabla} Y_{\text{steam}} \right) + Q_{\text{mass}}^{\text{drop}}, \tag{4}$$

  where $Y_{\text{steam}} = 1 - Y_{\text{air}}$ is steam mass concentration, Y_{air} is air mass concentration, D is the diffusion coefficient, and S_{c_t} is the Schmidt turbulent number ($S_{c_t} = 1$).
- The equation of state:

$$P = \frac{\rho_{\text{air}} R_0 T_{\text{air}}}{M}, \tag{5}$$

  where $R_0 = 8314.41$ J/kmol $\cdot$ K is the universal gas constant, M is the molecular weight, and T_{air} is the air temperature.

- The equation of the drop motion dynamics:

$$\frac{\partial V_{\text{drop}}}{\partial t} = \frac{\pi d_{\text{drop}}^2}{8 m_{\text{drop}}} C_D \rho_{\text{drop}} |V_{\text{air}} - V_{\text{drop}}| (V_{\text{air}} - V_{\text{drop}}) + g \left(1 - \frac{\rho_{\text{air}}}{\rho_{\text{drop}}}\right), \quad (6)$$

  where d_{drop} is the drop diameter, m_{drop} is the drop weight, ρ_{drop} is the drop density, V_{drop} is drop velocity, and C_D is the coefficient of resistance.
- The equation of mass conservation for the drop:

$$\frac{\partial m_{\text{drop}}}{\partial t} = -m^* \pi d_{\text{drop}}^2, \quad (7)$$

  where m^* is the steam injection parameter per drop surface unit.
- The equation of energy conservation for the drop:

$$\frac{\partial T_{\text{drop}}}{\partial t} = \left(\left[\text{Nu} \frac{\lambda_{\text{air}}}{d_{\text{drop}}} (T_{\text{air}} - T_{\text{drop}}) \right] - m^* q(T_{\text{drop}}) \right) \frac{6}{d_{\text{drop}} \rho_{\text{drop}} c_{p_{\text{drop}}}}, \quad (8)$$

  where $c_{p_{\text{drop}}}$ is the drop heat capacity, T_{drop} is the drop temperature, and Nu is the Nusselt number.
- The equation of turbulent energy:

$$\frac{\partial}{\partial t}(\rho_{\text{air}} K) + \bar{\nabla} \cdot (\rho_{\text{air}} V_{\text{air}} K) = \bar{\nabla} \cdot \left(\left(\mu + \frac{\mu_t}{\sigma} \right) \bar{\nabla} K \right) + \mu_t G - \rho_{\text{air}} \varepsilon, \quad (9)$$

  where σ is a constant, G determines the speed of turbulent energy generation, ε is the rate of turbulent energy dissipation, and K is turbulent energy.
  Given that the computational domain has a cylindrical geometry, the gas dynamic flow has a high speed, and the length is small and equals the distance from the injection of droplets through the nozzles to the barrier (experimental model), it is advisable to use the $K - \varepsilon$ turbulence model, which is applicable when the influence of inertial forces is large compared to viscosity forces.
- The equation of turbulent energy dissipation rate:

$$\frac{\partial}{\partial t}(\rho_{\text{air}} \varepsilon) + \bar{\nabla} \cdot (\rho_{\text{air}} V_{\text{air}} \varepsilon) = \bar{\nabla} \cdot \left(\left(\mu + \frac{\mu_t}{\sigma_\varepsilon} \right) \bar{\nabla} \varepsilon \right) + C_1 \frac{\varepsilon}{K} \mu_t G - C_2 f_1 \rho_{\text{air}} \frac{\varepsilon^2}{K}, \quad (10)$$

  where σ_ε, C_1 and C_2 are constants.

2.3 Parameters and criteria for optimization of gas dynamics calculation

The problem is solved in ANSYS CFX, as the initial and boundary conditions are given. We studied the solution convergence. Next, input and output parameters were parameterized in CFX and transferred to the ANSYS Workbench, a step that was necessary for the iterative start of ANSYS in the Globalizer optimization program.

The following ranges of input parameters were set:

1. $T_{\text{air}} = -30$ .. $0\,^{\circ}\text{C}$ for gas dynamic flow temperature;
2. $V_{\text{air}} = 10$ .. 270 m/s for gas dynamic flow rate;
3. $T_{\text{drop}}|_{l=0} = +5$ .. $+10\,^{\circ}\text{C}$ for the drop temperature at the initial moment of contact with the air flow;
4. $V_{\text{drop}} = 10$ .. 270 m/s for the drop velocity at the initial time of contact with the air flow.

The average drop diameter for injecting was taken equal to 20 μm, and did not change during computations.

We adopted the following output criteria for the optimization algorithm:

1. $T_{\text{drop}}|_{l=0} = -0.5$ .. $+0.5\,^{\circ}\text{C}$ for the drop temperature at the moment when it reaches the obstacle ($L = 2$ m);
2. $T_{\text{air}} \to \max$ for the maximum initial temperature of the gas dynamic flow.

The input parameter T_{air} is simultaneously an output criterion that approaches the maximum.

As we know, when integrating the multi-criteria parallel optimization IOSO PM program complex with ANSYS, it is possible to set the input parameter as an output optimization criterion only with additional program code associated with syntactic IOSO PM parameters, i.e. it is not foreseen within the core function of the optimization complex.

As regards the drop freezing, the air temperature cannot physically be above $+0.5\,^{\circ}\text{C}$, otherwise the drop will not be able to cool down to the temperature defined by the output criterion.

The optimization problem was solved with the generalized global optimization algorithm implemented in Globalizer. To allow for sorting the results of the Globalizers gas dynamics solution in ANSYS CFX, we wrote the respective functions, and parameterized the total count time (TotalTime) and the time step (TimeSteps).

The description of both the optimization algorithm and the Globalizer program system is given in the next section.

3 Global optimization with non-convex constraints

3.1 Problem statement

Let us consider the N-dimensional global optimization problem

$$\varphi(y^*) = \min\{\varphi(y) : y \in D,\ g_i(y) \le 0,\ 1 \le i \le m\}, \tag{11}$$

with search domain

$$D = \left\{y \in R^N : -2^{-1} \le y_j \le 2^{-1}, 1 \le j \le N\right\}. \tag{12}$$

This problem statement covers a large class of problems since the hyperinterval

$$S = \left\{y \in R^N : a_j \le y_j \le b_j, 1 \le j \le N\right\}$$

can be reduced to the hypercube (12) by linear transformation. The objective function $\varphi(y)$ (henceforth denoted by $g_{m+1}(y)$) and the left-hand sides $g_i(y),\ 1 \le i \le m$, of the constraints satisfy the Lipschitz conditions with constants $L_i,\ 1 \le i \le m+1$, respectively, and may be multiextremal. It is assumed that the functions $g_i(y)$ are defined and computable only at the points $y \in D$ satisfying the conditions

$$g_k(y) \le 0,\ 1 \le k < i. \tag{13}$$

Employing the continuous single-valued Peano curve $y(x)$ (*evolvent*) that maps the unit interval $[0,1]$ of the x-axis onto the N-dimensional domain (12), it is possible to find the minimum in the problem (11) by solving the one-dimensional problem

$$\varphi(y(x^*)) = \min\left\{\varphi(y(x)) : x \in [0,1],\ g_i(y(x)) \le 0,\ 1 \le i \le m\right\},$$

where, as it follows from(13), the functions $g_i(y(x))$ are defined and computable in the domains

$$Q_1 = [0,1],\ Q_{i+1} = \left\{x \in Q_i : g_i(y(x)) \le 0\right\},\ 1 \le i \le m.$$

These conditions allow for the introduction of a classification of the points $x \in [0,1]$ according to the number $\nu(x)$ of the constraints computed at this point. The *index* $\nu(x)$ can also be defined by the conditions

$$g_i(y(x)) \le 0,\ 1 \le i < \nu,\ g_\nu(y(x)) > 0,$$

where the last inequality is inessential if $\nu = m+1$.

The considered dimensionality reduction scheme juxtaposes a multidimensional problem with lipschitzian functions to a one-dimensional problem where the corresponding functions satisfy the uniform Hölder condition (see [18]), i.e.

$$|g_i(y(x')) - g_i(y(x''))| \le H_i \left|x' - x''\right|^{1/N},\ x', x'' \in [0,1],\ 1 \le i \le m+1.$$

Here N is the dimensionality of the initial multidimensional problem and the coefficients H_i are related with the Lipschitz constants L_i of the initial problem by the inequalities $H_i \le 2L_i\sqrt{N+3}$.

Thus, a *trial* at a point $x^k \in [0,1]$ executed at the k-th iteration of the algorithm will consist in the following sequence of operations:

- Determine the *image* $y^k = y(x^k)$ in accordance with the mapping $y(x)$.
- Compute the values $g_1(y^k), ..., g_\nu(y^k)$, where the index $\nu \le m$ is determined by the conditions

$$g_i(y^k) \le 0,\ 1 \le i < \nu,\ g_\nu(y^k) > 0,\ \nu \le m.$$

The occurrence of the first violation of the constraint terminates the trial. In the case when the point y^k is a feasible one, i.e. when $y(x^k) \in Q_{m+1}$, the trial includes the computation of the values of all the functions of the problems and the index is assumed to be $\nu = m+1$. The pair of values

$$\nu = \nu(x^k),\ z^k = g_\nu(y(x^k))$$

is a *trial result.*

3.2 Generalized global search algorithm

The rules that determine the work of the index method are the following.

The first trial is executed at an arbitrary internal point $x_1 \in (0,1)$. The selection of the point $x^{k+1},\ k \geq 1$, of any next trial is determined by the following rules.

Rule 1. Renumber the points $x^1, ..., x^k$ of the preceding trials by the lower indices in ascending order of coordinate values, i.e.

$$0 = x_0 < x_1 < \cdots < x_k < x_{k+1} = 1,$$

and juxtapose to them the values $z_i = g_\nu(y(x_i)),\ \nu = \nu(x_i),\ 1 \leq i \leq k$, computed at these points. The points $x_0 = 0$ and $x_{k+1} = 1$ are introduced additionally, while the values z_0 and z_{k+1} are not defined.

Rule 2. Classify the indices $i,\ 1 \leq i \leq k$, of the trial points according to the number of the problem constraints fulfilled at these points, by constructing the sets

$$I_\nu = \{i : 1 \leq i \leq k,\ \nu = \nu(x_i)\},\ 1 \leq \nu \leq m+1,$$

containing the numbers of all the points $x_i,\ 1 \leq i \leq k$, with the same values of ν. The end points $x_0 = 0$ and $x_{k+1} = 1$ are interpreted as the ones having indices equal to zero. An additional set, $I_0 = \{0, k+1\}$, corresponds to them.

Determine the maximum value of the index:

$$M = \max\{\nu(x_i),\ 1 \leq i \leq k\}.$$

Rule 3. Compute the current lower estimates,

$$\mu = \max\left\{\frac{|z_i - z_j|}{(x_i - x_j)^{1/N}},\ i, j \in I_\nu,\ i > j\right\},$$

for the unknown Hölder constants H_ν of the functions $g_\nu(y), 1 \leq \nu \leq m+1$. If a set I_ν contains less than two elements, or if μ_ν is equal to zero, then assume $\mu_\nu = 1$.

Rule 4. For all nonempty sets $I_\nu,\ 1 \leq \nu \leq m+1$, compute the estimates

$$z_\nu^* = \begin{cases} -\epsilon_\nu, & \nu < M, \\ \min\{g_\nu(y(x_i) : i \in I_\nu\}, & \nu = M, \end{cases}$$

where the nonnegative numbers $(\epsilon_1, ..., \epsilon_m)$ are parameters of the algorithm.

Rule 5. For each interval $(x_{i-1}, x_i),\ 1 \leq i \leq k+1$, compute the *characteristics* $R(i)$:

$$R(i) = 2\Delta_i - 4\frac{z_i - z_\nu^*}{r_\nu \mu_\nu},\ \nu = \nu(x_i) > \nu(x_{i-1}),$$

$$R(i) = \Delta_i + \frac{(z_i - z_{i-1})^2}{r_\nu^2 \mu_\nu^2 \Delta_i} - 2\frac{z_i + z_{i-1} - 2z_\nu^*}{r_\nu \mu_\nu},\ \nu = \nu(x_i) = \nu(x_{i-1}), \qquad (14)$$

$$R(i) = 2\Delta_i - 4\frac{z_{i-1} - z_\nu^*}{r_\nu \mu_\nu},\ \nu = \nu(x_{i-1}) > \nu(x_i),$$

where $\Delta_i = (x_i - x_{i-1})^{1/N}$. The values $r_\nu > 1,\ 1 \le \nu \le m+1$, are parameters of the algorithm. An appropriate selection of r_ν allows to consider the product $r_\nu \mu_\nu$ as an estimate of the Hölder constants $H_\nu,\ 1 \le \nu \le m+1$.

Rule 6. Find the interval (x_{t-1}, x_t) with the maximum characteristic

$$R(t) = \max\{R(i) : 1 \le i \le k+1\}. \tag{15}$$

Rule 7. Make the next trial at the midpoint of the interval (x_{t-1}, x_t) if the indices of the points x_{t-1} and x_t are not the same, i.e.

$$x^{k+1} = \frac{x_t + x_{t-1}}{2},\ \nu(x_{t-1}) \ne \nu(x_t).$$

Otherwise, make the trial at the point

$$x^{k+1} = \frac{x_t + x_{t-1}}{2} - \frac{\mathrm{sign}(z_t - z_{t-1})}{2r_\nu}\left[\frac{|z_t - z_{t-1}|}{\mu_\nu}\right]^N,\ \nu = \nu(x_{t-1}) = \nu(x_t). \tag{16}$$

We may take as termination condition the inequality $\Delta_t \le \epsilon$, where t is from (15) and $\epsilon > 0$ is the predefined accuracy.

Various modifications of this algorithm and the corresponding theory of convergence are given in [18–21].

The algorithm considered above is very flexible and allows for an efficient parallelization for shared memory, for distributed memory, and for accelerators [22–25].

4 Integration of Globalizer and ANSYS Workbench

This section contains a brief explanation of the Globalizer software system. The system expands the family of global optimization software that has been consistently developed at Nizhny Novgorod State University during the past several years.

The development of the system was based on the generalized global search algorithm that was described in the previous section. A major advantage of Globalizer is that the system is designed to solve time-consuming multiextremal optimization problems. The system efficiently uses modern high-performance computer systems to obtain the optimal solution within a reasonable time and at a reasonable cost.

The structural components of the Globalizer are the following blocks.

- Block 0 consists of the procedures for computing the function values (objective and constraints) for the optimization problem that is being solved; this is an external block with respect to the Globalizer system.
- Blocks 1–3 form the optimization subsystem and solve unconstrained (Block 1), constrained (Block 2) and multicriteria (Block 3) global optimization problems.
- Block 4 is a subsystem for accumulating and processing search information.

- Block 5 contains the dimensional reduction procedures based on evolvents; the optimization blocks solve the reduced (one-dimensional) optimization problems. Block 5 provides for interaction between the optimization blocks and the initial multidimensional optimization problem.
- Block 6 is responsible for managing the parallel processes while performing the global search (determining the optimal configuration of parallel processes, distributing the processes between computer elements, balancing computational loads, etc.).
- Block 7 is a common managing subsystem, which fully controls the entire computational process when solving global optimization problems.

In order to integrate Globalizer with ANSYS Workbench 13.0, we need to provide the call of an external calculator of function values (i.e. ANSYS) as Block 0. It is necessary to transfer the input parameter values of the ANSYS Workbench project, update the project and receive the output parameter values. The transfer of the parameters between the ANSYS Workbench and Globalizer was implemented by means of an IronPython script.

In the conducted experiments, computations were performed on a single cluster node. The parallelization of computations of the problem function values relied on ANSYS tools. The computation costs of executing the optimization algorithm in Globalizer (the choice of the next trial points, processing the trial results, etc.) were significantly less than those of computing the problem function values in ANSYS. Therefore, it was not necessary to parallelize the operations of the optimization module itself.

It is important to note that the integration of ANSYS and Globalizer allows for larger scale experiments to be performed with the use of several cluster nodes as well. In this case, search trials at different points of the search domain will be performed at all the nodes that are employed at each iteration of the method. Therefore, the results of the computations can be processed in Globalizer both synchronously and asynchronously. In the first case, the system waits until the computations on all nodes employed are completed. Then the processing of the results is performed, and the next iteration is started. This regime is preferred at equal computing time at any point of the search domain. In the second case, the results obtained at one of the nodes are processed immediately, and the next trial begins at this node. The asynchronous regime provides for the full load of the nodes to be utilized in the cases when trial times are different at different points of the search domain. The experiments performed earlier on test problems have demonstrated this approach to be promising [26]. Performing experiments of this kind on the solution of applied problems will be the subject of further investigations.

5 Optimization results

The Globalizer system allowed to construct a field of input parameter values that satisfy the above-mentioned (Sec. 2.3) restrictions of the gas dynamics problem (Fig. 1).

The total time spent on finding the solution of the optimization problem at the PNRPU high-performance computing complex was 48 hours.

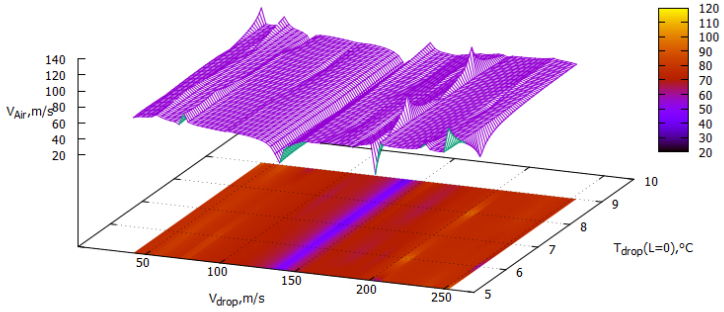

Fig. 1. Field of input parameter values that satisfy the output criteria of the optimization problem: V_{drop} — drop velocity, $T_{\text{drop}}|_{l=0}$ — drop temperature at the time of injection, V_{air} — air velocity

It was assumed that the energy-efficient modes of the CWT are those in which the gas dynamic flow temperature in the working section approaches the maximum at the drop temperature +0.5 °C when it reaches the barrier at a 2 m distance from the injection point:

$T_{\text{air}} \to \max$;

$T_{\text{drop}}|_{l=2\ \text{m}} = 0.5\,^{\circ}\text{C}$.

However, according to expert estimates, the ranges of permissible drop speed V_{drop} and temperature $T_{\text{drop}}|_{l=0}$ at the time of injection are the following:

$V_{\text{drop}} = 5$ .. 270 m/s;

$T_{\text{drop}|_{l=0}} = +5$ .. $+10$ °C.

As the optimization computations show, the values of drop speed and temperature in the energy-efficient modes of the CWT can vary within the following ranges (Fig. 1):

$V_{\text{drop}} = 42.37$ .. 237.63 m/s;

$T_{\text{drop}}|_{l=0} = +5$ .. $+9\,^{\circ}\text{C}$.

An analysis of the results of the computational optimization experiment (Fig. 1) showed that the range of drop velocities V_{drop} and drop temperatures $T_{\text{drop}}|_{l=0}$ corresponding to these modes of operation is narrower than the recommended pre-peer evaluations.

These findings identify the speed (for 26.32%) and temperature (for 20%) of the injection modes that produce icing in the work area based at the specified distance of the experimental model to the injection zone.

Fig. 2 shows that the variation of only two parameters, such as the speed of the gas dynamic flow (V_{air}) and the drop temperature at the time of injection through the nozzles ($T_{\text{drop}}|_{l=0}$), allows to achieve the desired value of the drop temperature (+0.5 °C) upon reaching the barrier (experimental model) when meeting the output optimization criterion $T_{\text{air}} \to +0.5\,^{\circ}\text{C}$. This may help to achieve energy-efficient modes in the CWT.

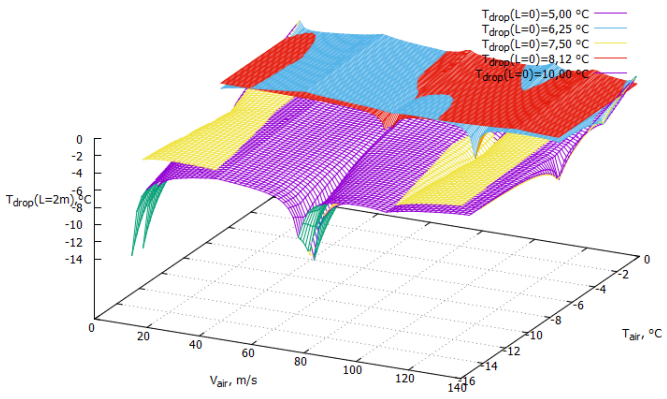

Fig. 2. Dependence of V_{air} (gas dynamic flow rate) and T_{air} (gas dynamic flow temperature) on $T_{\text{drop}}|_{l=2\text{ m}}$ (drop temperature when reaching the obstacle ($L = 2$ m)) for different values of $T_{\text{drop}}|_{l=0}$ (drop temperature at time of injection)

For example, in the given operation mode of the studied experimental model, by varying only technological parameters such as temperature and velocity of drops at the initial moment of contact with the gas flow, one can achieve an energy-efficient simulation of ice formation, except for a few bottlenecks in the drop velocity modes. Moreover, areas can be specified by applying a greater number of iterations (ANSYS starts) in the Globalizer optimization algorithm, which, of course, requires longer computation times.

6 Conclusions

1. As a result of the solution to the optimization problem, a combined region of speed and temperature parameters has been detected, as well as the air flow velocity at which the gas dynamic flow temperature in the working section approaches the maximum. This region is energy efficient, since it allows for icing without achieving significant negative airflow temperatures.
2. The possibility of implementing an energy efficient operation mode of the small-sized closed-loop CWT has been demonstrated by changing only technological parameters such as the initial drop temperature and velocity.

3. The integration of the Globalizer optimization system and the engineering software package ANSYS has been realized for the first time.
4. The Globalizer software package helps to find the best solutions at reasonable time and material costs.
5. The application of the Globalizer optimization software system made it possible to identify a fairly wide range of parameter combinations that allows to maintain the energy-efficient operation mode of the small-sized closed-loop CWT with sufficient accuracy for engineering practice ($\pm 1\,^{\circ}\mathrm{C}$).

References

1. Modorskii, V.Ya., Shevelev, N.A.: Research of aerohydrodynamic and aeroelastic processes on PNRPU HPC system. In: Vasily Fomin (Ed.) ICMAR 2016, AIP Conference Proceedings, vol. 1770, art. no. 020001 (2016); DOI: 10.1063/1.4963924
2. Shmakov, A.F., Modorskii, V.Y.: Energy Conservation in Cooling Systems at Metallurgical Plants. Metallurgist 59(9–10), 882–886 (2016); DOI: 10.1007/s11015-016-0188-8
3. Kalyulin, S.L., Modorskii, V.Ya., Paduchev, A.P.: Numerical design of the rectifying lattices in a small-sized wind tunnel. In: Vasily Fomin (Ed.) ICMAR 2016, AIP Conference Proceedings, vol. 1770, art. no. 030110 (2016); DOI: 10.1063/1.4964052
4. Afanasiev, V.A., Barsukov, V.S., Gofin, M.Ya., Zakharov, Yu.V., Strelchenko, A.N., Shalunov, N.P.: Experimental testing of spacecraft. MAI, Moscow (1994) [in Russian]
5. Goryachev, A.V., Mezhzil, E.K., Petrov, S.B., Syrov, V.A., Harlamov, A.V., Chivanov, S.V.: A way of ground testing objects of aircraft, subject to icing, and a device for its implementation. Patent RF, no. 2345345 (2007)
6. Klemenkov, G.P., Prihodko, Yu.M., Puzyrev, L.N., Haritonov, A.M.: Modelling of aircraft icing processes in aeroclimatic tubes. Thermophysics and Aeromechanics 15(4), 563–572 (2008) [in Russian]
7. Alekseenko, S.V., Prihodko, A.A.: Numerical simulation of icing cylinder and profile. Models review and calculation results. TsAGI Science Journal 44(6), 25–57 (2013) [in Russian]
8. Prihodko, A.A., Alekseenko, S.V.: Numerical simulation of icing aerodynamic surfaces in the presence of large overcooled water drops. JETP Letters 40(19), 75–82 (2014) [in Russian]
9. Hannat, R., Morency, F.: Numerical Validation of Conjugate Heat Transfer Method for Anti-/De-Icing Piccolo System. J. Aircr. 51(1), 104–116 (2014); DOI: 10.2514/1.c032078
10. Villalpando, F., Reggio, M., Ilinca, A.: Prediction of ice accretion and anti-icing heating power on wind turbine blades using standard commercial software. Energy 114, 1041–1052 (2016); DOI: 10.1016/j.energy.2016.08.047
11. Lynch, F.T., Khodadoust, A.: Effects of ice accretions on aircraft aerodynamics. Prog. Aeosp. Sci. 37(8), 669–767 (2001); DOI: 10.1016/s0376-0421(01)00018-5
12. Bragg, M.B., Broeren, A.P., Blumenthal, L.A.: Iced-airfoil aerodynamics. Prog. Aeosp. Sci. 41(5), 323–362 (2005); DOI: 10.4271/2003-01-2098
13. Modorskii, V.Ya., Sipatov, A.M., Babushkina, A.V., Kolodyazhny, D.Yu., Nagorny, V.S.: Modeling technique for the process of liquid film disintegration. In: Vasily Fomin (Ed.) ICMAR 2016, AIP Conference Proceedings, vol. 1770, art. no. 030109 (2016); DOI: 10.1063/1.4964051

14. Gaynutdinova, D.F., Modorsky, V.Y., Masich, G.F.: Infrastructure of Data Distributed Processing in High-Speed Process Research Based on Hydroelasticity Tasks. In: Sloot, P. (Ed.) YSC, Procedia Computer Science, vol. 66, pp. 556–563 (2015); DOI: 10.1016/j.procs.2015.11.063
15. Modorskii, V.Y., Gaynutdinova, D.F., Gergel, V.P., Barkalov, K.A.: Optimization in Design of Scientific Products for Purposes of Cavitation Problems. In: Simos T.E. (Ed.) ICNAAM 2015, AIP Conference Proceedings, vol. 1738, art. no. 400013 (2016); DOI: 10.1063/1.4952201
16. Modorskii, V.Y., Sokolkin, Y.V.: Dynamic Behavior of a thick-walled cylinder under pressurization. Izv. Vyss. Uchebnykh Zaved. Aviats. Tek. 4, 14–16 (2002)
17. Kozlova, A.V., Modorskii, V.Y., Ponik, A.N.: Modeling of Cooling Processes in the Variable Section Channel of a Gas Conduit. Russian Aeronautics 53(4), 401–407 (2010); DOI: 10.3103/s1068799810040057
18. Strongin, R.G., Sergeyev, Y.D.: Global Optimization with Non-Convex Constraints. Sequential and Parallel Algorithms. Kluwer Academic Publishers, Dordrecht (2000); DOI: 10.1007/978-1-4615-4677-1
19. Barkalov, K.A., Strongin, R.G.: A global optimization technique with an adaptive order of checking for constraints. Comput. Math. Math. Phys. 42(9), 1289–1300 (2002)
20. Gergel, V.P., Strongin, R.G.: Parallel computing for globally optimal decision making on cluster systems. Future Gener. Comput. Syst. 21(5), 673–678 (2005); DOI: 10.1016/j.future.2004.05.007
21. Sergeyev, Ya.D., Strongin, R.G., Lera, D.: Introduction to global optimization exploiting space-filling curves. Springer (2013); DOI: 10.1007/978-1-4614-8042-6
22. Barkalov, K., Ryabov, V., Sidorov, S.: Parallel Scalable Algorithms with Mixed Local-Global Strategy for Global Optimization Problems. In: Hsu, Ch., Malyshkin, V. (Eds.) MTPP 2010, LNCS, vol. 6083, pp. 232–240. Springer, Heidelberg (2010); DOI: 10.1007/978-3-642-14822-4_26
23. Barkalov, K., Gergel, V., Lebedev, I.: Use of Xeon Phi Coprocessor for Solving Global Optimization Problems. In: Malyshkin, V. (Ed.) PaCT 2015, LNCS, vol. 9251, pp. 307–318. Springer, Heidelberg (2015); DOI: 10.1007/978-3-319-21909-7_31
24. Barkalov, K., Gergel, V.: Parallel Global Optimization on GPU. J. Glob. Optim. 66(1), 3–20 (2016); DOI: 10.1007/s10898-016-0411-y
25. Barkalov, K., Gergel, V., Lebedev, I.: Solving Global Optimization Problems on GPU Cluster. In: Simos T.E. (Ed.) ICNAAM 2015, AIP Conference Proceedings, vol. 1738, art. no. 400006 (2016); DOI: 10.1063/1.4952194
26. Gergel, V., Sidorov, S.: A Two-Level Parallel Global Search Algorithm for Solution of Computationally Intensive Multiextremal Optimization Problems. In: Malyshkin, V. (Ed.) PaCT 2015, LNCS, vol. 9251, pp. 505–515. Springer, Heidelberg (2015); DOI: 10.1007/978-3-319-21909-7_49